Title: The structural architecture of an α-synuclein toxic oligomer.

Authors: Jaime Santos[1], Jorge Cuellar[2]†, Irantzu Pallarès[1]†, Emily J Byrd[3], Alons Lends[4], Fernando Moro[5], Muhammed Bilal Abdul-Shukkoor[4], Jordi Pujols[1], Lorea Velasco-Carneros[5], Frank Sobott[3], Daniel E Otzen[6], Antonio N Calabrese[3], Arturo Muga[5], Jan Skov Pedersen[7], Antoine Loquet[4], Jose María Valpuesta[2], Sheena E Radford[3] and Salvador Ventura[1]*.

Affiliations:

[1]Institut de Biotecnologia i Biomedicina and Departament de Bioquímica i Biologia Molecular, Universitat Autònoma de Barcelona; Bellaterra, Barcelona, Spain.

[2]Department of Macromolecular Structures, Centro Nacional de Biotecnología (CNB-CSIC); Madrid, Spain.

[3]Astbury Centre for Structural Molecular Biology, School of Molecular and Cellular Biology, Faculty of Biological Sciences, University of Leeds; Leeds, LS2 9JT, UK.

[4]Univ. Bordeaux, CNRS, Bordeaux INP, CBMN, UMR 5248, IECB; Pessac, France.

[5]Instituto Biofisika (UPV/EHU, CSIC) y Dpto. de Bioquímica y Biología Molecular, Facultad de Ciencia y Tecnología, Universidad del País Vasco; Barrio Sarriena S/N, 48940 Leioa, Spain.

[6]Interdisciplinary Nanoscience Center (iNANO) and Department of Molecular Biology and Genetics, Aarhus University; Gustav Wieds Vej 14, 8000 Aarhus C, Denmark.

[7]Interdisciplinary Nanoscience Center (iNANO) and Department of Chemistry, Aarhus University; Gustav Wieds Vej 14, 8000 Aarhus C, Denmark.

*Corresponding author: salvador.ventura@uab.es

†Authors contributed equally

Abstract: Oligomeric species populated during α-synuclein aggregation are considered key drivers of neurodegeneration in Parkinson's disease. However, their structure and the molecular determinants driving their conversion to fibrils remain elusive. In this work, we determined the symmetry and architecture of α-synuclein oligomers, dissecting the conformational properties of individual chains within these toxic assemblies. We demonstrate that the NAC domain is insufficient to promote oligomer to fibril conversion; instead, this transition is controlled by a short α-synuclein N-terminal motif. A missense mutation causing early-onset Parkinson's disease remodels this N-terminal region conformation, which results in a population of long-lived oligomers less susceptible to disaggregation by the human Hsp70 machinery. Our results provide a structural understanding of oligomer to amyloid conversion and identify targets for therapeutic intervention.

One sentence summary:

α-Synuclein oligomers are symmetric and well-organized particles with a short N-terminal region controlling fibril conversion.

Main text:

α-Synuclein (αS) is a 140 residue intrinsically disordered protein whose aggregation into amyloid fibrils is implicated in the onset of Parkinson's disease and other synucleinopathies (*1–3*). The aggregation landscape of αS is characterized by the early formation of transient oligomeric species that later convert into amyloid fibrils, whose accumulation is a defining hallmark of brain pathology (*4–8*). Oligomers are considered responsible for the gain-of-toxic function associated with αS aggregation (*9*, *10*) and, therefore, offer promising targets for therapeutics and diagnosis (*11*). However, knowledge of αS oligomer structure is limited, and the underlying mechanism for oligomer to fibril conversion is yet to be elucidated. Significant efforts have been devoted to gathering structural information on kinetically trapped αS oligomers (*8*, *12–14*), but their highly dynamic nature (*13*) makes this a challenging task.

Tight molecular binders, such as antibodies, can stabilize and reduce the conformational heterogeneity of target proteins, facilitating 3D structure determination of otherwise intractable proteins and their complexes. Here we mimicked this approach and used the amphipathic 22-residue peptide phenol-soluble modulin α3 (PSMα3), a nanomolar binder of αS oligomers (K_D = 6.67 nM; 1:1 PSMα3 per αS molecule at saturation) (*15*), as a tool to investigate their structural nature.

Architecture of αS oligomers

Isolated oligomer preparations were generated by incubating 800 μM of ^{13}C, ^{15}N labeled monomeric αS for 20 hours at 37 °C quiescently, followed by centrifugation-based fractionation as previously described (*12*). Oligomer-PSMα3 complexes were prepared by incubating oligomers with a 3-fold molar excess of PSMα3 and subsequent removal of the unbound peptide. Magic-angle spinning (MAS) solid-state nuclear magnetic resonance (ssNMR) cross-polarization (CP) and insensitive nuclei enhanced by polarization transfer (INEPT) were used to measure ^{13}C signals in rigid (CP) and mobile (INEPT) molecular segments of αS oligomers in the absence or presence of PSMα3. Peptide binding to oligomers increased the CP signal and CP/INEPT ratio, indicating oligomer rigidification upon interaction (**Fig. 1A; and Fig. S1A and B**). Nevertheless, the chemical shifts in the CP- and INEPT-based 2D spectra remained largely unchanged (**Fig. 1B and Fig. S1C**), ruling out major structural alterations upon PSMα3 binding. The unique set of resonances in the 2D CP-based spectrum of oligomers revealed a

monomorphic rigid core that we assigned as residues 70 to 89 based on previous studies (*16*) of αS fibrils (**Fig. S1D**). The assignments agree with those reported for a previously characterized toxic αS oligomer (*13*). Hence, 60% of residues seem to share a similar secondary structural context in oligomers and fibrils, with chemical shift differences < 1 ppm in both alpha (Cα) and beta (Cβ) carbons (**Fig. S1D and Table S1**).

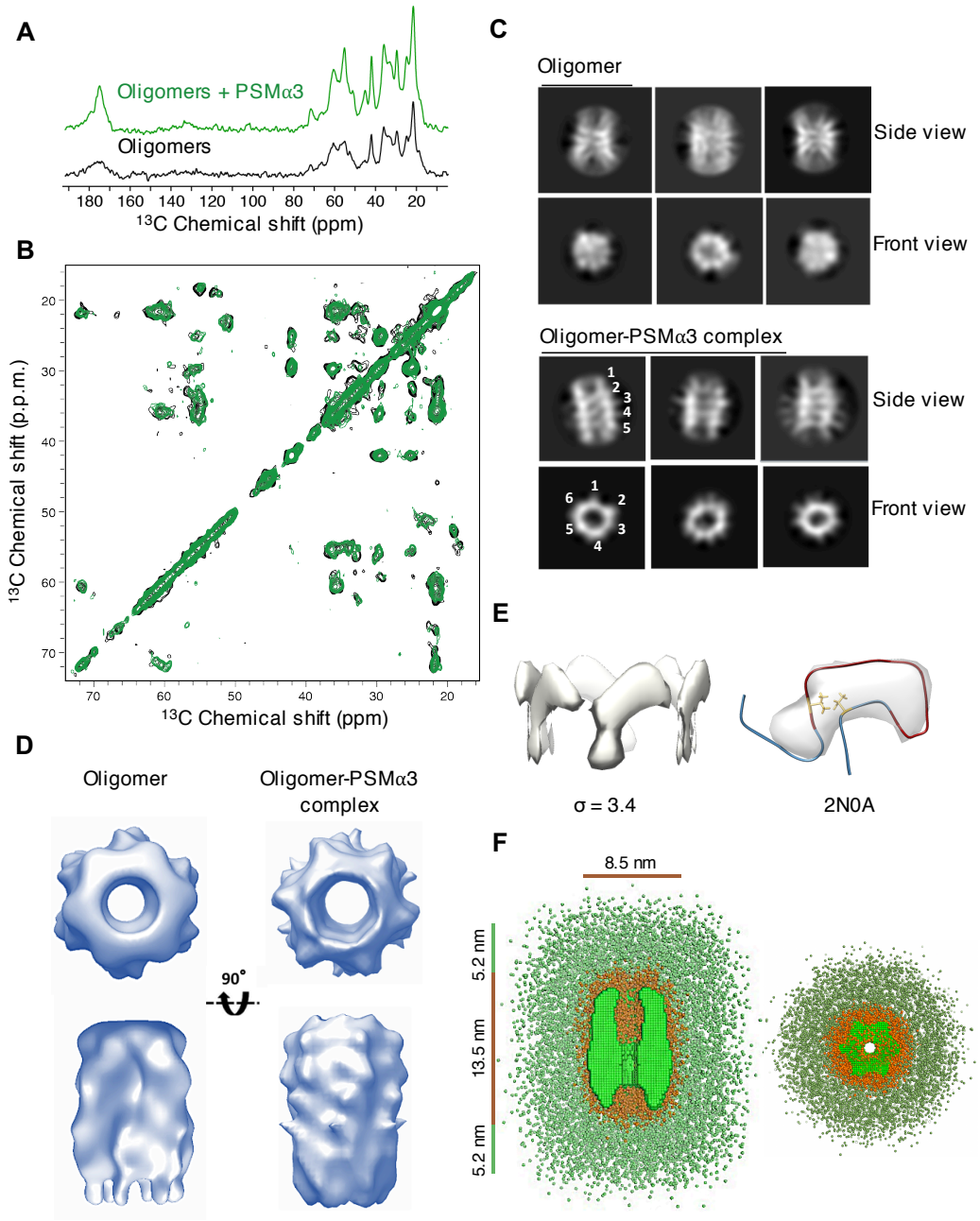

Fig. 1. Structural characterization of αS oligomers. (**A**) 1D ^{13}C spectra of oligomers and oligomers in complex with PSMα3 detected using cross-polarization (CP) ssNMR. (**B**) 2D ^{13}C-^{13}C PDSD correlation spectra (mixing time of 50 ms) of oligomers (black) and oligomers + PSMα3 (green). (**C**) 2D cryoEM classes of oligomers and oligomers in complex with PSMα3. The observed symmetry and architecture are labeled with numbers. (**D**) 3D reconstruction, six-fold symmetry

imposed, in the absence and presence of PSMα3 with resolutions of 16 Å and 16.7 Å, respectively. (**E**) The left panel shows the visualization of an αS oligomer CryoEM density at a high visualization threshold (σ = 3.4). The right panel shows the overlay of the same density with the NAC domain from resolved αS fibrils (PDB: 2N0A). Residues assigned as the rigid core of αS oligomers by ssNMR are shown in red (70-89). Valine 71 and threonine 92 in yellow. (**F**) Two views of the SAXS-based 3D reconstruction of αS oligomers. The compact core (orange) is surrounded by an outer disordered shell (green). The cryoEM density map is shown inside the oligomer core (bright green).

Consistent with the ssNMR data, PSMα3 binding reduced the conformational heterogeneity of αS oligomers as judged by negative stain transmission electron microscopy (nsEM) images (**Fig. S2A and B**). We exploited this increase in structural order for cryo-electron microscopy (cryoEM) 3D density reconstruction. In the presence of PSMα3, two structural features were evident in the 2D classes generated during 3D reconstruction: i) end-on views showed a 6-fold symmetry, also visible in the nsEM, ii) side views revealed an arrangement of five layers (**Fig. 1C**). These two traits were also apparent in the PSMα3-free oligomers. A 3D reconstruction of the two sets of particles was performed and, in both cases, the obtained structure displayed a cylindrical architecture with a central hollow core (**Fig. S2C, D and E**). Despite their limited resolution, both 3D reconstructions evidenced a 6-fold symmetry (**Fig. 1C and Fig. S2B, D and E**). This symmetry was applied to improve the quality of the two 3D reconstructions to a final resolution of 16 Å and 16.7 Å (**Fig. 1D**).

A 6-fold symmetry and 5-layer organization provide the structural context to accommodate the 30 αS monomers known to form these oligomers (*8*, *12*, *15*). The stacking of five hexameric rings best explains the EM data, while the single set of resonances evidenced by ssNMR suggests that all αS subunits have equivalent conformations and chemical environments. Our data thus demonstrate unequivocally that these αS oligomers have a well-defined and symmetric internal architecture.

Increasing the sigma (σ) value of the 3D reconstruction reveals the region of highest density (**Fig. S3**). At high sigma values (σ = 3.4), we observed a relatively well-defined region of cryoEM density, with a shape similar to a hammerhead (**Fig. 1E**), which we hypothesized should correspond to the residues identified as the rigid core by ssNMR. Given the similarities in the chemical shifts of αS oligomers and fibrils (PDB entry 2N0A (*16*)), we overlaid the structure of αS subunits in 22 different fibril structures with the cryoEM density of αS oligomers (**Fig. S4**). The 2N0A Greek key motif fitted the oligomer density (**Fig. 1E**), and was observed in several independent protofilament subunits, including fibrils extracted from multiple system atrophy

(MSA) patients (**Fig. S4**). In the Greek key motif of eight of the analyzed fibril structures, residues 71 and 92 face each other at < 10 Å distance (Cα to Cα) (**Fig. S4**). We tested whether this pattern is consistent with the oligomer structure by engineering a disulfide bond (design described in Methods) to covalently link these residues (**Fig. S5A**). Oxidized V71C-T92C monomers assembled into oligomers identical in size, morphology, and secondary structure content to those of wild-type (WT) αS (**Fig. S5**), demonstrating that a structural constraint < 7 Å between Val71 and Thr92 Cα is compatible with the proposed oligomer structure. These data suggest that the Greek key arrangement is already imprinted in the oligomer and maintained upon oligomer-to-fibril conversion.

By leveraging the cryoEM map, we used small-angle X-ray scattering (SAXS) to build a structural model that includes the dynamic and disordered αS regions averaged out in cryoEM reconstructions (**Fig. 1F; Fig. S6A and Table S2**). The oligomer core visible in the cryoEM maps is surrounded by an outer shell of disordered tails, resulting in an oligomer radius of gyration of 76.1 ± 0.3 Å, a dimension consistent with previous reports (*8*, *17*). Additionally, we confirmed that αS oligomers have an aggregation number close to 30 (**Table S2**). Surprisingly, our experimental data fitted better to a model with a single random coil chain per monomer, including 48% of αS residues, rather than two (**Fig. S6B**), as would be expected if both the N- and C-terminal domains remained fully disordered. Consistent with this, hydrogen-deuterium exchange-mass spectrometry (HDX-MS) analysis confirmed that the N-terminal domain became protected against deuterium uptake in the oligomer compared with the monomer. In contrast, the HDX protection in the C-terminal region remained unchanged (**Fig. 2A and Fig. S7**). The enhanced protection in the N-terminal domain is endowed by contacts between different residues in this domain, as well as by interdomain interactions of the N-terminal and NAC regions, as identified by crosslinking mass spectrometry (XL-MS) (**Fig. S8A and Supplementary Data 1**).

The N-terminal P1 and P2 regions control oligomer-to-fibril conversion

XL-MS of the oligomer-PSMα3 complex revealed that peptide binding is mediated by four regions in the N-terminal domain; residues 1-6, 24-32 and the previously identified P1 and P2 regions (residues 36-42 and 45-57, respectively) (*18*) (**Fig. 2B and Supplementary Data 2**). Additionally, HDX-MS indicated that the P1 and P2 regions (40-61) become protected from deuterium uptake upon PSMα3 binding (**Fig. 2B, Fig. S7 and S8B**). This suggests that, despite

being protected from HDX in the oligomer, the N-terminal region is still accessible and available for interactions.

We recently described that the P1 and P2 regions (**Fig. 2B**) act as 'master controllers' of αS amyloid formation *in vitro* and in *C. elegans* (*18*, *19*). The deletion of P1 (ΔP1) inhibits αS amyloid formation, in agreement with our previous results, with the deletion of P2 (ΔP2) also retarding amyloid formation under the conditions used here (*18*, *19*) (**Fig. 2C and Fig. S9**). The fact that PSMα3 stalls amyloid formation by blocking oligomer-to-fibril conversion (*15*) and the evidence that PSMα3 targets these αS motifs, suggest that the P1 and P2 regions are involved in this pivotal stage of amyloid formation. As expected, few low molecular weight species (isolation of this fraction is described in materials and methods) were visible at the endpoint of the amyloid assembly assay of WT αS (**Fig. 2D**). By contrast, oligomers identical in shape and size to WT oligomers were the primary components for ΔP1 and ΔP2 (**Fig. 2D and Fig. S2**). Similar results were obtained with a double deletion of P1 and P2 in tandem (ΔΔ) (**Fig. S10A**). The modulation of amyloid formation by the P1 region has been shown to be dependent on specific residues (*19*). Hence we characterized two αS variants, Y39A and S42A, which we found previously to mimic the ΔP1 phenotype (*19*). Consistent with our prior results, the Y39A and S42A amino acid substitutions inhibited αS amyloid formation to different extents (**Fig. S10B and C**). In both cases, oligomers with a WT-like architecture were the predominant species at the time points of maximal inhibition, indicating an impact in the oligomer to fibril transition (**Fig. S10B and C**). The WT αS and S42A proteins differ only in a single hydroxymethyl group, evidencing the precise control that small sequence changes exert in oligomer to fibril conversion.

To discard oligomer presence being intrinsic to any αS inhibited reaction, we characterized an N-terminal truncated variant (ΔN11) whose reduced amyloid assembly is due to decreased secondary nucleation (*7*, *20*). Importantly, deletion of the N-terminal eleven residues inhibited amyloid formation, but oligomers were marginal in the low-molecular weight fraction (**Fig. S10D**).

Our data argue that P1 and P2 are not necessary for αS oligomerization, but instead serve as 'master controllers' of oligomer-to-fibril conversion. The sequence dependence of this transition and the HDX protected, but PSMα3-accessible, nature of P1 and P2 in the oligomer suggest that this αS motif samples structured or partially structured conformations critical for amyloid formation, emphasizing the essential role these core-flanking regions play in generating the amyloid fold.

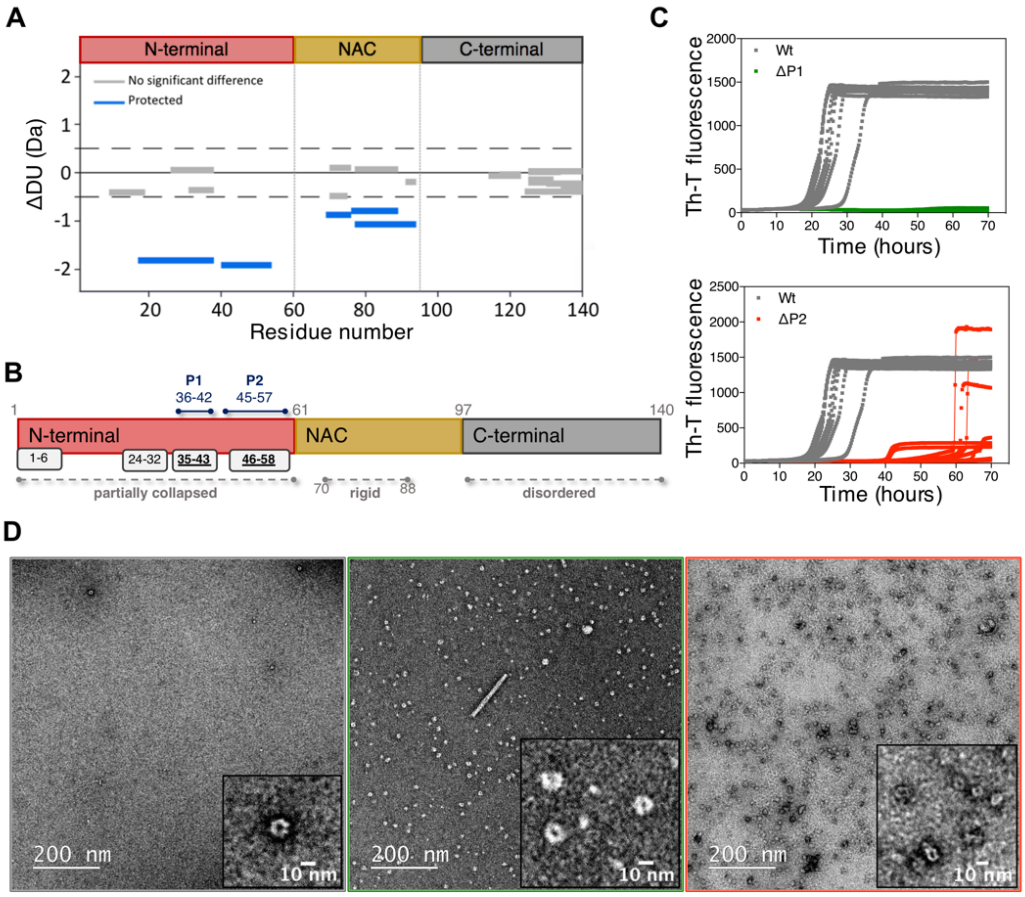

Fig. 2. Dynamics of the N-terminal domain and contribution to amyloid formation. (**A**) Wood's plots showing the difference in deuterium uptake (ΔDU) between αS monomers and oligomers by HDX-MS at the 60 seconds exposure timepoint to deuterium. Peptides colored in blue are protected from exchange in αS oligomers, suggesting they are less solvent-exposed. (**B**) Schematic representation of the conformational state of each αS domain. White boxes represent PSMα3 binding sites in the N-terminal domain identified by XL-MS; bold underlined numbers indicate PSMα3 binding sites that overlay between XL-MS and HDX-MS. P1 and P2 regions (*18*) are labeled in blue. (**C**) Kinetics of amyloid formation of the WT, ΔP1 and ΔP2 variants monitored using Th-T fluorescence. (**D**) Representative nsEM images of the oligomeric fraction of the WT, ΔP1 and ΔP2 variants (left, center and right, respectively) isolated at the endpoint of the assembly reaction

The hereditary mutation G51D impairs N-terminal mediated oligomer-to-fibril conversion and chaperone-assisted disaggregation.

The oligomer architecture we describe here also provides a structural context to rationalize the clustering of mutations associated with familial PD around P2 sequence (positions 46, 50, 51, and 53). According to this model, changes in the side chains of these residues can influence N-terminal domain conformational dynamics, oligomer's physicochemical properties and its ability to convert into amyloid fibrils. The familial G51D mutation best exemplifies this effect, since it results in structurally diverse oligomers characterized by a distinctive α-helical component, as

previously reported (*21*) and shown here (**Fig. 3A**). HDX-MS reveals that this point-mutation causes significant deprotection from deuterium uptake specifically in the N-terminal region of the oligomers (**Fig. S7 and Fig. S11**). We observed that the delayed aggregation of G51D αS is associated with the presence of WT-like oligomers at the timepoint of maximal difference (t = 28 hours) with the WT kinetics (**Fig. 3B and C**). The G51D variant exemplifies how a disease-associated mutation in P2 elicits a structural rearrangement of the N-terminal domain of the oligomer, including P1, which further impacts oligomer-to-fibril conversion.

The N-terminal domain of monomeric αS encompasses two binding sites (residues 1-10 and 37-43) for Hsp70 (*22*, *23*). WT and G51D oligomers display conformational differences in this region, which might impact how these αS assemblies interact with, and are processed by the Hsp70-based human disaggregation system (*24*). Accordingly, while WT αS oligomers are efficiently disaggregated into monomers by the synergistic action of Hsc70, DNAJB1 and Apg2 chaperones, the G51D oligomers show a significantly greater degree of resistance to Hsc70-mediated disaggregation (**Fig. 3D and Fig. S12**). Hsc70-mediated processing of αS oligomers is therefore critically dependent on the conformational organization of the N-terminal domain in the oligomer. Thus, under normal physiological conditions, αS oligomerization can be effectively counteracted by the chaperone machinery. However, familial mutations, like G51D, impacting the dynamics of the N-terminal regions involved in oligomer-to-fibril transition and Hsc70 interaction would lead to the accumulation of long-lived, toxic (*21*), oligomers that are not efficiently processed by the human disaggregase machinery. This might be why these mutations cause PD onset at ages at which protein homeostasis is still preserved.

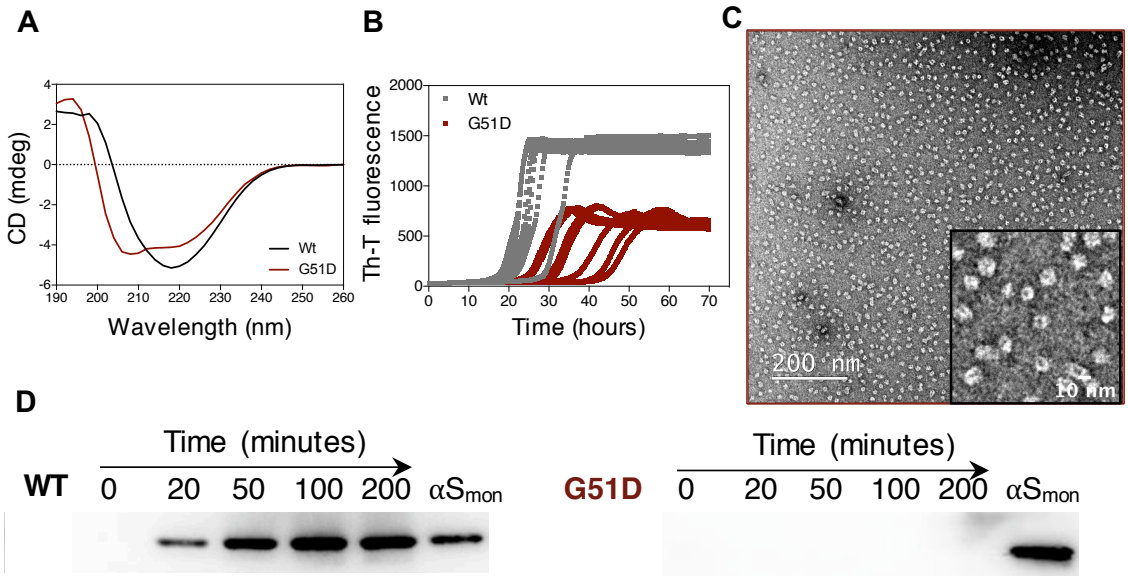

Fig. 3. The effect of the familial G51D mutation on αS amyloid and oligomer formation and disaggregation by molecular chaperones. (**A**) Circular dichroism spectra of kinetically trapped oligomers of G51D (dark red) and WT αS (black). (**B**) Assembly kinetics of G51D into amyloid fibrils monitored using ThT fluorescence. (**C**) Representative nsEM micrographs of the G51D oligomeric fraction after 28 hours of assembly. (**D**) Disaggregation of WT (left) and G51D (right) oligomers by the human Hsp70 chaperone disaggregation machinery at different time points analyzed by native-PAGE and western blot. 2 µM of monomeric αS (αS_{mon}) was added as a control.

Discussion

Overall, we show that the here studied αS oligomers have a symmetric and well-defined core molecular architecture, mainly sustained by the rigid NAC domain in a conformation structurally akin to that observed in many αS amyloid fibrils. Nevertheless, the NAC region is not sufficient to drive the oligomer to fibril conversion, likely because of its rigidity and burial in the assembly. Instead, the N-terminal flanking region, and especially the P1 and P2 sequences therein, modulate oligomer-to-fibril conversion, with the dynamic but partially collapsed P1-P2 region becoming engaged in sequence-specific contacts responsible for this structural transition (**Fig. 4**). This motif is solvent accessible and targetable in the oligomeric state, offering the opportunity to develop molecular binders for therapeutic and diagnostic use, as exemplified here using the PSMα3 peptide. The G51D oligomer polymorphism and its decreased susceptibility to chaperone-mediated disaggregation suggest a molecular basis for understanding why this and possibly other point mutations clustering at P2 are associated with familial PD.

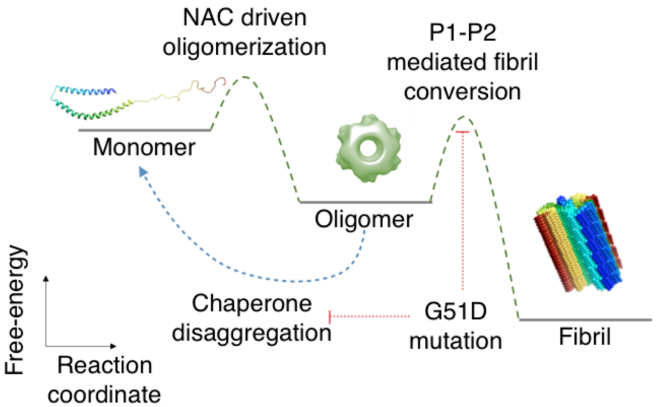

Fig. 4. Schematic representation of the αS aggregation landscape.

References:

1. M. G. Spillantini, M. L. Schmidt, V. M. Lee, J. Q. Trojanowski, R. Jakes, M. Goedert, Alpha-synuclein in Lewy bodies. *Nature*. **388**, 839–840 (1997).
2. M. H. Polymeropoulos, C. Lavedan, E. Leroy, S. E. Ide, A. Dehejia, A. Dutra, B. Pike, H. Root, J. Rubenstein, R. Boyer, E. S. Stenroos, S. Chandrasekharappa, A. Athanassiadou, T. Papapetropoulos, W. G. Johnson, A. M. Lazzarini, R. C. Duvoisin, G. Di Iorio, L. I. Golbe, R. L. Nussbaum, Mutation in the alpha-synuclein gene identified in families with Parkinson's disease. *Science*. **276**, 2045–2047 (1997).
3. M. Goedert, R. Jakes, M. G. Spillantini, The Synucleinopathies: Twenty Years On. *J Parkinsons Dis*. **7**, S51–S69 (2017).
4. N. Cremades, S. I. A. Cohen, E. Deas, A. Y. Abramov, A. Y. Chen, A. Orte, M. Sandal, R. W. Clarke, P. Dunne, F. A. Aprile, C. W. Bertoncini, N. W. Wood, T. P. J. Knowles, C. M. Dobson, D. Klenerman, Direct observation of the interconversion of normal and toxic forms of α-synuclein. *Cell*. **149**, 1048–1059 (2012).
5. E. Zurlo, P. Kumar, G. Meisl, A. J. Dear, D. Mondal, M. M. A. E. Claessens, T. P. J. Knowles, M. Huber, In situ kinetic measurements of α-synuclein aggregation reveal large population of short-lived oligomers. *PLoS One*. **16**, e0245548 (2021).
6. A. J. Dear, T. C. T. Michaels, G. Meisl, D. Klenerman, S. Wu, S. Perrett, S. Linse, C. M. Dobson, T. P. J. Knowles, Kinetic diversity of amyloid oligomers. *Proc Natl Acad Sci U S A*. **117**, 12087–12094 (2020).
7. X. Yang, B. Wang, C. L. Hoop, J. K. Williams, J. Baum, NMR unveils an N-terminal interaction interface on acetylated-α-synuclein monomers for recruitment to fibrils. *Proc Natl Acad Sci U S A*. **118**, e2017452118 (2021).
8. N. Lorenzen, S. B. Nielsen, A. K. Buell, J. D. Kaspersen, P. Arosio, B. S. Vad, W. Paslawski, G. Christiansen, Z. Valnickova-Hansen, M. Andreasen, J. J. Enghild, J. S. Pedersen, C. M. Dobson, T. P. J. Knowles, D. E. Otzen, The role of stable α-synuclein oligomers in the molecular events underlying amyloid formation. *J Am Chem Soc*. **136**, 3859–3868 (2014).
9. B. Winner, R. Jappelli, S. K. Maji, P. A. Desplats, L. Boyer, S. Aigner, C. Hetzer, T. Loher, M. Vilar, S. Campioni, C. Tzitzilonis, A. Soragni, S. Jessberger, H. Mira, A. Consiglio, E. Pham, E. Masliah, F. H. Gage, R. Riek, In vivo demonstration that alpha-synuclein oligomers are toxic. *Proc Natl Acad Sci U S A*. **108**, 4194–4199 (2011).
10. J. M. Froula, M. Castellana-Cruz, N. M. Anabtawi, J. D. Camino, S. W. Chen, D. R. Thrasher, J. Freire, A. A. Yazdi, S. Fleming, C. M. Dobson, J. R. Kumita, N. Cremades, L. A. Volpicelli-Daley, Defining α-synuclein species responsible for Parkinson's disease phenotypes in mice. *J Biol Chem*. **294**, 10392–10406 (2019).
11. N. Bengoa-Vergniory, R. F. Roberts, R. Wade-Martins, J. Alegre-Abarrategui, Alpha-synuclein oligomers: a new hope. *Acta Neuropathol*. **134**, 819–838 (2017).
12. S. W. Chen, S. Drakulic, E. Deas, M. Ouberai, F. A. Aprile, R. Arranz, S. Ness, C. Roodveldt, T. Guilliams, E. J. De-Genst, D. Klenerman, N. W. Wood, T. P. J. Knowles, C. Alfonso, G. Rivas, A. Y. Abramov, J. M. Valpuesta, C. M. Dobson, N. Cremades, Structural characterization of toxic oligomers that are kinetically trapped during α-synuclein fibril formation. *Proc Natl Acad Sci U S A*. **112**, E1994-2003 (2015).
13. G. Fusco, S. W. Chen, P. T. F. Williamson, R. Cascella, M. Perni, J. A. Jarvis, C. Cecchi, M. Vendruscolo, F. Chiti, N. Cremades, L. Ying, C. M. Dobson, A. De Simone, Structural basis of membrane disruption and cellular toxicity by α-synuclein oligomers. *Science*. **358**, 1440–1443 (2017).
14. N. Cremades, S. W. Chen, C. M. Dobson, Structural Characteristics of α-Synuclein Oligomers. *Int Rev Cell Mol Biol*. **329**, 79–143 (2017).
15. J. Santos, P. Gracia, S. Navarro, S. Peña-Díaz, J. Pujols, N. Cremades, I. Pallarès, S.

Ventura, α-Helical peptidic scaffolds to target α-synuclein toxic species with nanomolar affinity. *Nat Commun*. **12**, 3752 (2021).
16. M. D. Tuttle, G. Comellas, A. J. Nieuwkoop, D. J. Covell, D. A. Berthold, K. D. Kloepper, J. M. Courtney, J. K. Kim, A. M. Barclay, A. Kendall, W. Wan, G. Stubbs, C. D. Schwieters, V. M. Y. Lee, J. M. George, C. M. Rienstra, Solid-state NMR structure of a pathogenic fibril of full-length human α-synuclein. *Nat Struct Mol Biol*. **23**, 409–415 (2016).
17. A. Farzadfard, J. N. Pedersen, G. Meisl, A. K. Somavarapu, P. Alam, L. Goksøyr, M. A. Nielsen, A. F. Sander, T. P. J. Knowles, J. S. Pedersen, D. E. Otzen, The C-terminal tail of α-synuclein protects against aggregate replication but is critical for oligomerization. *Commun Biol*. **5**, 123 (2022).
18. C. P. A. Doherty, S. M. Ulamec, R. Maya-Martinez, S. C. Good, J. Makepeace, G. N. Khan, P. van Oosten-Hawle, S. E. Radford, D. J. Brockwell, A short motif in the N-terminal region of α-synuclein is critical for both aggregation and function. *Nat Struct Mol Biol*. **27**, 249–259 (2020).
19. S. M. Ulamec, R. Maya-Martinez, E. J. Byrd, K. M. Dewison, Y. Xu, L. F. Willis, F. Sobott, G. R. Heath, P. van Oosten Hawle, V. L. Buchman, S. E. Radford, D. J. Brockwell, Single residue modulators of amyloid formation in the N-terminal P1-region of α-synuclein. *Nat Commun*. **13**, 4986 (2022).
20. P. Kumari, D. Ghosh, A. Vanas, Y. Fleischmann, T. Wiegand, G. Jeschke, R. Riek, C. Eichmann, Structural insights into α-synuclein monomer-fibril interactions. *Proc Natl Acad Sci U S A*. **118**, e2012171118 (2021).
21. C. K. Xu, M. Castellana-Cruz, S. W. Chen, Z. Du, G. Meisl, A. Levin, B. Mannini, L. S. Itzhaki, T. P. J. Knowles, C. M. Dobson, N. Cremades, J. R. Kumita, The Pathological G51D Mutation in Alpha-Synuclein Oligomers Confers Distinct Structural Attributes and Cellular Toxicity. *Molecules*. **27**, 1293 (2022).
22. B. M. Burmann, J. A. Gerez, I. Matečko-Burmann, S. Campioni, P. Kumari, D. Ghosh, A. Mazur, E. E. Aspholm, D. Šulskis, M. Wawrzyniuk, T. Bock, A. Schmidt, S. G. D. Rüdiger, R. Riek, S. Hiller, Regulation of α-synuclein by chaperones in mammalian cells. *Nature*. **577**, 127–132 (2020).
23. A. S. Wentink, N. B. Nillegoda, J. Feufel, G. Ubartaitė, C. P. Schneider, P. De Los Rios, J. Hennig, A. Barducci, B. Bukau, Molecular dissection of amyloid disaggregation by human HSP70. *Nature*. **587**, 483–488 (2020).
24. A. Franco, P. Gracia, A. Colom, J. D. Camino, J. Á. Fernández-Higuero, N. Orozco, A. Dulebo, L. Saiz, N. Cremades, J. M. G. Vilar, A. Prado, A. Muga, All-or-none amyloid disassembly via chaperone-triggered fibril unzipping favors clearance of α-synuclein toxic species. *Proc Natl Acad Sci U S A*. **118**, e2105548118 (2021).

Acknowledgements:

Authors thank the cryoEM CNB-CSIC facility (CRIOMECORR project ESFRI-2019-01-CSIC-16), the services of the CNB-CSIC Mass Spectrometry facility, the Biomolecular mass spectrometry facility (UL) funded by the BBSRC (BB/M012573/1), the Microscopy Services (UAB), the Laboratori de Luminiscència i Espectroscòpia de Biomolècules (UAB) and the Biophysical and Structural Chemistry Platform at IECB, CNRS UAR 3033, INSERM US001. We thank James Ault for technical support with HDX-MS experiments and David Brockwell for illuminating discussions on the P1 region of αS.

Funding:

Spanish Ministry of Economy and Competitiveness (MINECO) grant BIO2016-78310-R and BIO2017-91475-EXP (SV)

Spanish Ministry of Science and Innovation (MICINN) grant PID2019-105017RB-I00 (SV)

MICINN grant PID2019-105872 GB-I00 (JMV)

MICINN grant PID2019-111068GB-I00 (AM)

ICREA-Academia 2015 (SV)

MICINN doctoral grant FPU17/01157 (JS)

Early postdoc mobility project SNSF P2EZP2_184258 (AL)

Basque Government grant IT1201-19 (FM)

BBSRC BB/M011151/1 grant (EJB)

Sir Henry Dale Fellowship jointly funded by Wellcome and the Royal Society 220628/Z/20/Z (ANC)

Royal Society grant RGS\R2\222357 (ANC)

University Academic fellowship from the University of Leeds (ANC)

Royal Society Research Professorship RSRP/R1/211057 (SER)